

1 **Biallelic variants in *DAP3* result in reduced assembly of the mitoribosomal small**
2 **subunit with altered intrinsic and extrinsic apoptosis and a Perrault syndrome-**
3 **spectrum phenotype**

4
5 Thomas B. Smith^{*},^{1,2} Robert Kopajtich^{*} ^{3,4} Leigh A.M. Demain,^{1,2} Alessandro Rea,^{1,2} Huw B.
6 Thomas,^{1,2} Manuel Schiff,^{5,6} Christian Beetz,⁷ Shelagh Joss,⁸ Gerard S. Conway,⁹
7 Anju Shukla¹⁰, Mayuri Yeole¹⁰, Periyasamy Radhakrishnan¹⁰, Hatem Azzouz,¹¹ Amel Ben
8 Chehida,¹¹ Monique Elmaleh-Bergès,¹² Ruth I.C. Glasgow,¹³ Kyle Thompson,¹⁴ Monika
9 Oláhová,^{14,15} Langping He,¹⁶ Emma M. Jenkinson,^{1,2} Amir Jahic,¹⁷ Inna A. Belyantseva,¹⁸
10 Melanie Barzik,¹⁸ Jill E. Urquhart,^{1,2} James O' Sullivan,^{1,2} Simon G. Williams,^{1,2} Sanjeev S.
11 Bhaskar,^{1,2} Samantha Carrera,¹⁹ Alexander J.M. Blakes,^{1,2} Siddharth Banka,^{1,2} Wyatt W.
12 Yue,²⁰ Jamie M. Ellingford,^{1,2,21} Henry Houlden,²² DDD Study,²³ Kevin J. Munro,²⁴ Thomas
13 B. Friedman,¹⁸ Robert W. Taylor,^{14,16} Holger Prokisch^Δ, ^{3,4} Raymond T. O'Keefe^Δ, ^{1,2}
14 William G. Newman^Δ ^{1,2}

15
16 1. Division of Evolution, Infection and Genomics, School of Biological Sciences, The
17 University of Manchester, Manchester, M13 9PL, UK

18 2. Manchester Centre for Genomic Medicine, St Mary's Hospital, The University of
19 Manchester NHS Foundation Trust, Manchester, M13 9WL, UK

20 3. Institute of Human Genetics, Computational Health Center, Helmholtz Zentrum
21 München, Neuherberg, 85764, Germany.

22 4. Institute of Human Genetics, School of Medicine, Technical University of Munich,
23 Munich, 81675, Germany.

24 5. Université Paris Cité, Reference Center for Mitochondrial Disorders (CARAMMEL) and
25 Reference Center Inborn Error of Metabolism, Department of Pediatrics, Necker-Enfants

26 Malades Hospital, APHP, Filiale G2M, Paris, France

NOTE: This preprint reports new research that has not been certified by peer review and should not be used to guide clinical practice.

- 27 6. Inserm UMR_S1163, Institut Imagine, Université Paris Cité, Paris, France.
- 28 7. Centogene GmbH, Rostock, Germany.
- 29 8. West of Scotland Centre for Genomic Medicine, Queen Elizabeth University Hospital,
30 Glasgow G51 4TF, UK.
- 31 9. Institute for Women's Health, University College London, London, United Kingdom.
- 32 10. Department of Medical Genetics, Kasturba Medical College, Manipal, Manipal
33 Academy of Higher Education, Manipal, India.
- 34 11. Service de pédiatrie et des maladies métaboliques héréditaires, CHU la Rabta, 1007
35 Jabberi, Tunis, Tunisia.
- 36 12. Service de Radiologie Pédiatrique, Hôpital Robert-Debré, APHP, Paris, France.
- 37 13. Department of Medical Biochemistry and Biophysics, Karolinska Institutet, 171 65,
38 Stockholm, Sweden
- 39 14. Mitochondrial Research Group, Clinical and Translational Research Institute, Faculty
40 of Medical Sciences, Newcastle University, Newcastle upon Tyne, NE2 4HH, UK
- 41 15. Department of Applied Sciences, Faculty of Health & Life Sciences, Northumbria
42 University, Newcastle upon Tyne, UK.
- 43 16. NHS Highly Specialised Service for Rare Mitochondrial Disorders, Newcastle upon
44 Tyne Hospitals NHS Foundation Trust, Newcastle upon Tyne, NE1 4LP, UK
- 45 17. Institute of Diagnostic Laboratory Medicine, Clinical Chemistry and Pathobiochemistry,
46 Charité - Universitätsmedizin Berlin, Berlin, Germany.
- 47 18. Laboratory of Molecular Genetics, National Institute on Deafness and Other
48 Communication Disorders, National Institutes of Health, Bethesda, MD, 20892-3729, USA
- 49 19. Genome Editing Unit, The University of Manchester, Manchester, M13 9PT, UK.
- 50 20. Newcastle University Biosciences Institute, Medical School, Framlington Place,
51 Newcastle upon Tyne, NE2 4HH, UK
- 52 21. Genomics England, London, UK.

53 22. Department of Molecular Neuroscience, UCL Queen Square Institute of Neurology,
54 London, United Kingdom.

55 23. Wellcome Trust Sanger Institute, Cambridge, UK.

56 24. Manchester Centre for Audiology and Deafness (ManCAD), School of Health
57 Sciences, The University of Manchester, Manchester, UK.

58

59 * **These authors contributed equally.**

60 ^Δ **Senior author.**

61

62 Correspondence to

63 william.newman@manchester.ac.uk

64 rokeefe@manchester.ac.uk

65 **Abstract**

66 The mitoribosome synthesizes 13 protein subunits of the oxidative phosphorylation system
67 encoded by the mitochondrial genome. The mitoribosome is composed of 12S rRNA, 16S
68 rRNA and 82 mitoribosomal proteins encoded by nuclear genes. To date, variants in 12
69 genes encoding mitoribosomal proteins are associated with rare monogenic disorders, and
70 frequently show combined oxidative phosphorylation deficiency. Here, we describe five
71 unrelated individuals with biallelic variants in the *DAP3* nuclear gene encoding
72 mitoribosomal small subunit 29 (MRPS29), with variable clinical presentations ranging
73 from Perrault syndrome (sensorineural hearing loss and ovarian insufficiency) to an early
74 childhood neurometabolic phenotype. Assessment of respiratory chain function and
75 proteomic profiling of fibroblasts from affected individuals demonstrated reduced MRPS29
76 protein levels, and consequently decreased levels of additional protein components of the
77 mitoribosomal small subunit, associated with a combined complex I and IV deficiency.
78 Lentiviral transduction of fibroblasts from affected individuals with wild-type *DAP3* cDNA
79 increased *DAP3* mRNA expression, and partially rescued protein levels of MRPS7,
80 MRPS9 and complex I and IV subunits, demonstrating the pathogenicity of the *DAP3*
81 variants. Protein modelling suggested that *DAP3* disease-associated missense variants
82 can impact ADP binding, and *in vitro* assays demonstrated *DAP3* variants can
83 consequently reduce both intrinsic and extrinsic apoptotic sensitivity, *DAP3* thermal
84 stability and *DAP3* GTPase activity. Our study presents genetic and functional evidence
85 that biallelic variants in *DAP3* result in a multisystem disorder of combined oxidative
86 phosphorylation deficiency with pleiotropic presentations, consistent with mitochondrial
87 dysfunction.

88

89 **Keywords**

90 DAP3, mitochondria, mitoribosome, MRPS29, rare disease, Perrault syndrome,
91 sensorineural hearing loss, ovarian insufficiency, leukodystrophy, mitoribosomal small
92 subunit

93

94 **Introduction**

95 Mitochondrial ribosomes (mitoribosomes) are present in the mitochondria of all eukaryotic
96 cells. The function of the mitoribosome is to facilitate translation of mitochondrial mRNAs
97 that exclusively encode components of the oxidative phosphorylation (OXPHOS)
98 complexes. The mitoribosome consists of a small subunit (SSU) comprised of 30
99 mitoribosomal proteins (MRPs) and a 12S rRNA that binds mRNA and tRNA to ensure
100 accurate initiation and decoding, and a large subunit (LSU) comprised of 52 MRPs, 16S
101 rRNA, and mt-tRNA^{Val} that links a nascent polypeptide to the inner mitochondrial
102 membrane via the OXA1L insertase¹⁻⁴. Formation of the mitoribosome is achieved
103 through sequential steps. For the LSU, these steps can be divided into early, intermediate
104 and late, whereas for the SSU these steps are only divided into early and late⁵. Several
105 human diseases are caused by germline variants in genes encoding mitoribosome
106 proteins or assembly factors⁶ (Table S1). Death-associated protein 3 (DAP3), also known
107 as mitochondrial ribosomal small subunit 29 (MRPS29), is a GTP-binding protein of the
108 mitoribosome SSU. The precise function of DAP3 within the mitoribosome remains
109 unclear, but it is assembled into the SSU at an early stage, interacts extensively with the
110 12S rRNA and may associate with components of the inner mitochondrial membrane^{5,7}.
111 DAP3 was initially identified as a pro-apoptotic protein⁸ involved in interferon- γ -, tumor
112 necrosis factor (TNF)- α - and FAS-induced cell death⁹. DAP3 can also influence
113 mitochondrial fission by modulating dynamin related protein phosphorylation, with DAP3
114 depletion resulting in decreased mitochondrial protein synthesis, ATP production and
115 autophagy¹⁰. Recently, DAP3 has also been linked to regulation of RNA editing and

116 splicing in the context of cancer ^{11,12}, further highlighting *DAP3*'s broad range of functions.

117 To date, no *DAP3* variants have been reported in association with monogenic disorders.

118

119 Perrault syndrome is an ultra-rare, autosomal recessive condition characterized by

120 sensorineural hearing loss (SNHL) in both sexes and primary ovarian insufficiency (POI) in

121 46, XX karyotype females (Pallister and Opitz, 1979). Neurological features are present in

122 some affected individuals, often associated with brain white matter changes ¹³. As well as

123 being clinically heterogeneous with variable degrees of severity, progression and age of

124 onset of SNHL and POI in affected individuals ¹⁴, Perrault syndrome is remarkably

125 genetically heterogeneous for such a rarely reported condition. To date, biallelic variants in

126 eight genes are definitively associated with Perrault syndrome (Table S2). However,

127 biallelic variants in other genes, including *RMND1*, *PEX6*, *MRPS7*, and *MRPL50* ^{15–18} have

128 been identified in individuals with some features of Perrault syndrome, with a blended

129 phenotype accounting for some diagnoses ¹⁹.

130

131 Despite this rich genetic architecture, potentially up to 50% of individuals with Perrault

132 syndrome do not have a molecular diagnosis. Similarly, a large fraction of individuals with

133 a suspected mitochondrial disease remain without a molecular diagnosis even after

134 genome sequencing. Here, we present five individuals each with biallelic variants in *DAP3*

135 (Table 1) with accompanying functional data providing evidence that *DAP3* variants result

136 in decreased protein stability, reduced apoptotic sensitivity and impaired mitoribosomal

137 assembly, leading to deficits consistent with mitochondrial disease. This study further

138 underscores the importance of mitoribosome proteins in auditory and ovarian function.

139

140 **Material and methods**

141 **Recruitment of research subjects**

142 Individuals with clinical features of Perrault syndrome were recruited from the UK,
143 Tajikistan, Tunisia and India through GeneMatcher ²⁰, the Deciphering Developmental
144 Disorders (DDD) project ²¹ and Centogene (<https://www.centogene.com/>). Informed
145 consent for DNA analysis was obtained from study participants according to local
146 institutional ethics requirements. Individuals (and/or their legal guardians) recruited in this
147 study gave informed consent for their participation. The individual research studies
148 received ethical approval by the National Health Service Ethics Committee (16/WA/0017
149 and 10/H0305/83) and The University of Manchester.

150 **Whole exome sequencing**

151 WES was performed on DNA extracted from lymphocytes from individual F1:II-1. The
152 SureSelect Human All Exon V5 Panel (Agilent Technologies) was used for library
153 preparation and sequencing was performed on the HiSeq 2500 (Illumina) as previously
154 described ²². Exome data for affected individuals in families F2-4 were generated as
155 previously described ^{21,23,24}. For F5:II-1, the TWIST Human Core Exome Plus exome
156 capture kit was used, with the Illumina platform utilized for sequencing.

157

158 **Identification, amplification and confirmation of the DAP3 fusion product**

159 A 135 Kb deletion encompassing *DAP3* was identified using the ExomeDepth (v1.1.6)
160 software package ^{25,26}. Read depth was approximately 0.5 times the aggregated depth
161 indicating a single allele deletion. The fusion product and breakpoint region were
162 confirmed in the F1 proband by Sanger sequencing using ABI big Dye v3.1 (Thermo
163 Fisher Scientific Inc, Waltham, MA, USA) sequencing technology. Primers (Table S3) were
164 designed to target polymorphisms distinguishing the two segmental duplications where the
165 deletion breakpoints were situated.

166

167 **Maintenance of human dermal fibroblasts**

168 Fibroblasts were cultured in high glucose Dulbecco's Modified Eagle's Medium (Sigma)
169 with 10% foetal bovine serum (Sigma) and 10 mL/L penicillin-streptomycin (Sigma), at
170 37°C / 5% CO₂.

171

172 **Fibroblast respiratory chain activity assays**

173 Respiratory chain complex activities were assessed in fibroblasts from affected individuals
174 F1 and F4, as outlined previously ²⁷.

175

176 **RNA extraction, cDNA synthesis and RT-qPCR**

177 Fibroblasts were seeded into 6-well plates (Corning) and were incubated at 37°C / 5% CO₂
178 until approximately 90% confluent. Following one phosphate buffered saline (PBS) wash,
179 RNA was extracted from cells using TRI-Reagent® (Sigma), according to manufacturer's
180 instructions. Total RNA was converted to cDNA using the GoScript™ (Promega) Reverse
181 Transcription System with random hexamers (Thermo Fisher) according to manufacturer's
182 instructions, normalizing all RNA concentrations to the lowest measured.

183

184 RT-qPCR reactions to assess 12S:16S ratios and mt-DNA gene expression were
185 performed using 2 µM primer pairs, PowerUp™ SYBR™ Green Master Mix (Thermo
186 Fisher) and 1 µL template cDNA. Primer sequences are listed in Table S3. The
187 StepOnePlus Real-Time PCR System (Applied Biosystems) was used to measure
188 fluorescence, using the Comparative CT reaction cycle programme. $2^{-\Delta\Delta CT}$ values were
189 calculated by the accompanying StepOnePlus v2.3 data analysis package, normalizing to
190 *ACTB* (NM_001101.5) expression. 12S:16S ratios were calculated by totaling the 12S and
191 16S RQ values, then dividing the specific RQ value by the total value. All reactions were
192 run in triplicate in 96-well plates. Data was presented using GraphPad Prism 9 throughout
193 this study.

194 **Expression and purification of recombinant wild-type and variant *DAP3***

195 Purified DNA fragments comprised of truncated *DAP3* (*DAP3* Δ 46) wild-type or disease-
196 associated variants from amplified cDNA were inserted into the pMAL-c4X plasmid (New
197 England Biolabs) at the multiple cloning site downstream of maltose binding protein
198 (MBP), alongside a C-terminal 6x His-tag using NEBuilder[®] HiFi DNA Assembly Master
199 Mix (New England Biolabs) according to the manufacturer's instructions. A pMAL-c4x
200 vector containing MBP fused to only the 6x His-tag was also produced for a negative
201 control. All primer sequences for site-directed mutagenesis and mutagenic
202 oligonucleotides are listed in Tables S3-S4. Following confirmation via Sanger sequencing
203 (Eurofins Genomics), plasmids were transformed into Rosetta 2 (DE3) *E. coli* cells
204 (Novagen) and cultured in Overnight Express TB medium (Novagen) at 19°C for 72 hours.
205 Pellets were resuspended in lysis/wash buffer comprised of 20 mM Tris-Cl pH 7.4, 150
206 mM NaCl, 0.1 mM DTT, 20 mM imidazole (Sigma) and 15% glycerol. All purified proteins
207 were captured and separated by affinity chromatography utilizing the 6x His-tag. His-
208 tagged proteins were then eluted in lysis/wash buffer containing 250 mM imidazole.
209 Selected fractions were then dialyzed overnight at 4°C in 20 mM Tris-HCl pH 8, 200 mM
210 NaCl, 2 mM DTT and 15% glycerol. Proteins were then centrifuged at 17,000 x g for 10
211 minutes at 4°C, and the supernatants were frozen at -80°C.

212

213 **GTPase assays**

214 GTPase assays were conducted using the GTPase-Glo[™] Assay (Promega) in white
215 opaque 96-well plates (Greiner Bio-One) in accordance with the manufacturer's guidelines.
216 A final concentration of 5 μ M *DAP3* protein, 5 μ M GTP and 1 mM DTT was selected for
217 use in the GTPase reaction, which ran for one hour at room temperature. Luminescence of
218 residual GTP converted to ATP was measured using the BioTek Synergy H1 microplate
219 reader (Agilent) 10 minutes after addition of detection buffer, with reactions conducted in

220 duplicate over three independent assays. Residual GTP was calculated as a percentage
221 using a no protein control, with an MBP-His protein control ran in parallel to ensure
222 observed GTPase activity was DAP3-specific. Data was collected using Gen5 v2.07
223 software (Agilent).

224

225 **Proteomic analysis**

226 Fibroblasts from F1:II-1 and F4:II-1 were processed and analyzed through an established
227 proteomics pipeline to quantify the protein levels of both DAP3, and components of the
228 mitoribosome and respiratory chain complexes. Two parameters of the protocol previously
229 described²⁸ have been modified: Peptide fractionation was carried out using high pH
230 reverse phase instead of trimodal mixed-mode chromatography and TMT-labeling was
231 carried using TMT 11-plex instead of TMT 10-plex reagent. For data normalization,
232 quantification and detection of aberrant protein expression, a denoising autoencoder
233 based approach OUTRIDER2 was employed (termed PROTRIDER in Kopajtich *et al.*
234 2021).

235

236 **Apoptosis assays**

237 Control and affected individual fibroblasts were seeded in opaque, white 96 well plates
238 (Greiner Bio-One) at a density of 15,000 cells per well and incubated for 24 hours at 37°C
239 / 5% CO₂. Cells were treated with either 1 µM staurosporine (Cayman) for 4.5 hours to
240 induce the intrinsic apoptotic pathway, 0.05 µg/mL or 0.5 µg/mL TNF-α (Sigma) in
241 combination with 10 µg/mL cycloheximide (Cayman) for 24 hours to induce the extrinsic
242 apoptosis pathway, or with suitable controls (0.01% DMSO and 10 µg/mL cycloheximide).
243 Apoptotic activity was quantified using the Caspase-Glo® 3/7 Assay System (Promega),
244 as per manufacturer's instructions.

245

246 **Thermal shift assay (TSA)**

247 TSA was performed using the Protein Thermal Shift™ Dye Kit (Fisher Scientific) as per the
248 manufacturer's instructions in 96 well plates using the StepOnePlus Real-Time PCR
249 System. 1 µg of recombinant MBP-DAP3 protein was subjected to melt-curve analysis in
250 triplicate, progressing from 25°C to 90°C with a 1% temperature ramp rate. Melting
251 temperature (T_m) was derived by plotting melt curves of temperature against fluorescence
252 intensity, selecting the temperature at which peak fluorescent intensity was detected.

253

254 **Lentiviral transduction of *DAP3* cDNA**

255 A third-generation lentiviral construct was assembled using VectorBuilder, inserting full-
256 length *DAP3* cDNA upstream of T2A:EGFP under the control of an EF1α short form (EFS)
257 promoter. Following confirmatory Sanger sequencing and lentiviral packaging, fibroblasts
258 from affected individuals and controls were seeded in 12-well plates at a density of 40,000
259 cells per well for RNA extraction, or into T25 flasks (Corning) at a density of 200,000 cells
260 per flask for immunoblotting. Cells were immediately transduced in combination with 5
261 µg/mL Polybrene (Sigma), then incubated for 24 hours at 37°C and 5% CO₂. Cells were
262 washed three times with PBS, then growth media was replaced. After 72 hours post-
263 transduction, cells were washed 3 times with PBS and processed as required. Subsequent
264 RNA extraction, cDNA synthesis and qPCR analysis were conducted as described above.

265

266 **SDS-PAGE and immunoblotting**

267 Cells were pelleted and lysed in 50 µl Pierce™ IP Lysis Buffer (Thermo Scientific)
268 supplemented with 50x protease inhibitor cocktail (Promega) on ice, then agitated for 30
269 minutes at 4°C and centrifuged at 13,000 rpm for 15 minutes. Samples were mixed 1:1
270 with 2X SDS-PAGE sample buffer and heated to linearise protein, then ran on a 4-12%
271 polyacrylamide gel made in-house at 180V for 60 minutes alongside the Precision Plus

272 Protein Dual Color Standards (Bio-Rad) ladder. Proteins were transferred onto a 0.45µm
273 PVDF blotting membrane (GE Healthcare) using a Trans-Blot Semi-Dry Transfer Cell
274 System (Bio-Rad) for 30 minutes at 20V. The membrane was washed with 1x TBS-Tween
275 and blocked with 5% milk for 1 hour with agitation. Primary antibodies specific to MRPS7
276 (Abcam, ab224442), MRPS9 (Abcam, ab187906), the five antibodies provided in the Total
277 OXPHOS Human WB Antibody Cocktail (ATP5A, UQCRC2, SDHB, COXII, and NDUFB8)
278 (Abcam, ab110411) and beta-actin (ProteinTech; 20536-1-AP, 66009-1-Ig) were incubated
279 overnight at 4°C in block with agitation. Dilutions were 1:200 (MRPS7, MRPS9), 1:500
280 (Total OXPHOS) and 1:5000 (beta-actin) respectively. After washing, secondary
281 antibodies were incubated with the membrane for 1 hour at 1:10,000, and were as follows:
282 IRDye® 800CW Goat anti-Rabbit IgG (LI-COR, 926-32211) and IRDye® 680RD Goat anti-
283 Mouse IgG antibody (LI-COR, 926-68070). Blots were washed in TBS-Tween and
284 visualised with the LICOR Odyssey FC imaging system using the 600, 700 and 800
285 channels. Quantification was achieved using LICOR Image Studio and beta-actin was
286 used to normalise band intensities.

287

288 **DAP3 localisation in mouse organ of Corti**

289 The NIH Animal Care and Use Committee approved protocol #1263-15 to T.B.F. for
290 mouse use. C57Bl/6J mice at postnatal day 3 (P3), P10, and P14 were euthanized, the
291 cochleae were removed and fixed with 4% paraformaldehyde in PBS for 2 hours at room
292 temperature (RT). The samples were microdissected, and the organ of Corti was
293 permeabilized with 0.5% Triton-X100 in PBS for 30 minutes followed by three 10 minute
294 washes with 1X PBS. Nonspecific binding sites were blocked with 5% normal goat serum
295 and 2% BSA in PBS for 1 hour at RT. Samples were incubated for 2 hours at RT with
296 primary antibodies (Table S5) in blocking solution, followed by several rinses with PBS.
297 Then, samples were incubated with secondary antibodies (Table S5) for 30 minutes at RT,

298 washed several times with PBS, mounted with ProLongGold Antifade staining reagent with
299 DAPI (Molecular Probes, Invitrogen, Carlsbad, CA, USA) and examined using a LSM780
300 confocal microscope (Zeiss Microimaging Inc, Oberkochen, Germany) equipped with 63X,
301 1.4 N.A. objective.

302 **Mouse organ of Corti Helios Gene Gun transfection**

303 Inner ear sensory epithelium cultures were prepared from P1 C57Bl/6J mouse organ of
304 Corti and transfected with plasmid DNA using the gene gun method as previously
305 described²⁹. Briefly, the organ of Corti spiral was dissected in Leibowitz cell culture
306 medium (Invitrogen, Carlsbad, CA, USA) and attached to a glass-bottom Petri dish
307 (MatTek, Ashland, MA, USA), coated with rat tail collagen and maintained at 37°C and 5%
308 CO₂ in DMEM supplemented with 7% FBS for 1–3 days. Cultures were transfected using a
309 Helios gene gun (Bio-Rad, Hercules, CA, USA). Gold particles of 1.0 µm diameter (Bio-
310 Rad, Hercules, CA, USA) were coated with DAP3-EGFP plasmid DNA at a ratio of 2 µg of
311 plasmid DNA to 1 mg of gold particles and precipitated onto Tefzel tubing, which was cut
312 into individual cartridges containing approximately 1 µg of plasmid DNA. Samples were
313 bombarded with gold particles from one cartridge per culture by using 110-120 psi of
314 helium. After an additional 8 hours to 4 days in culture, samples were fixed in 4%
315 paraformaldehyde and stained using the same method as the tissue samples above.

316

317 **Statistical analysis**

318 Statistical analyses were accomplished using GraphPad Prism 9 (GraphPad) software,
319 performing one-way or two-way ANOVAs using either Dunnett's or Tukey's multiple
320 comparisons tests where appropriate, as indicated in the figure legends. Statistical
321 significance was defined as a *p*-value < 0.05.

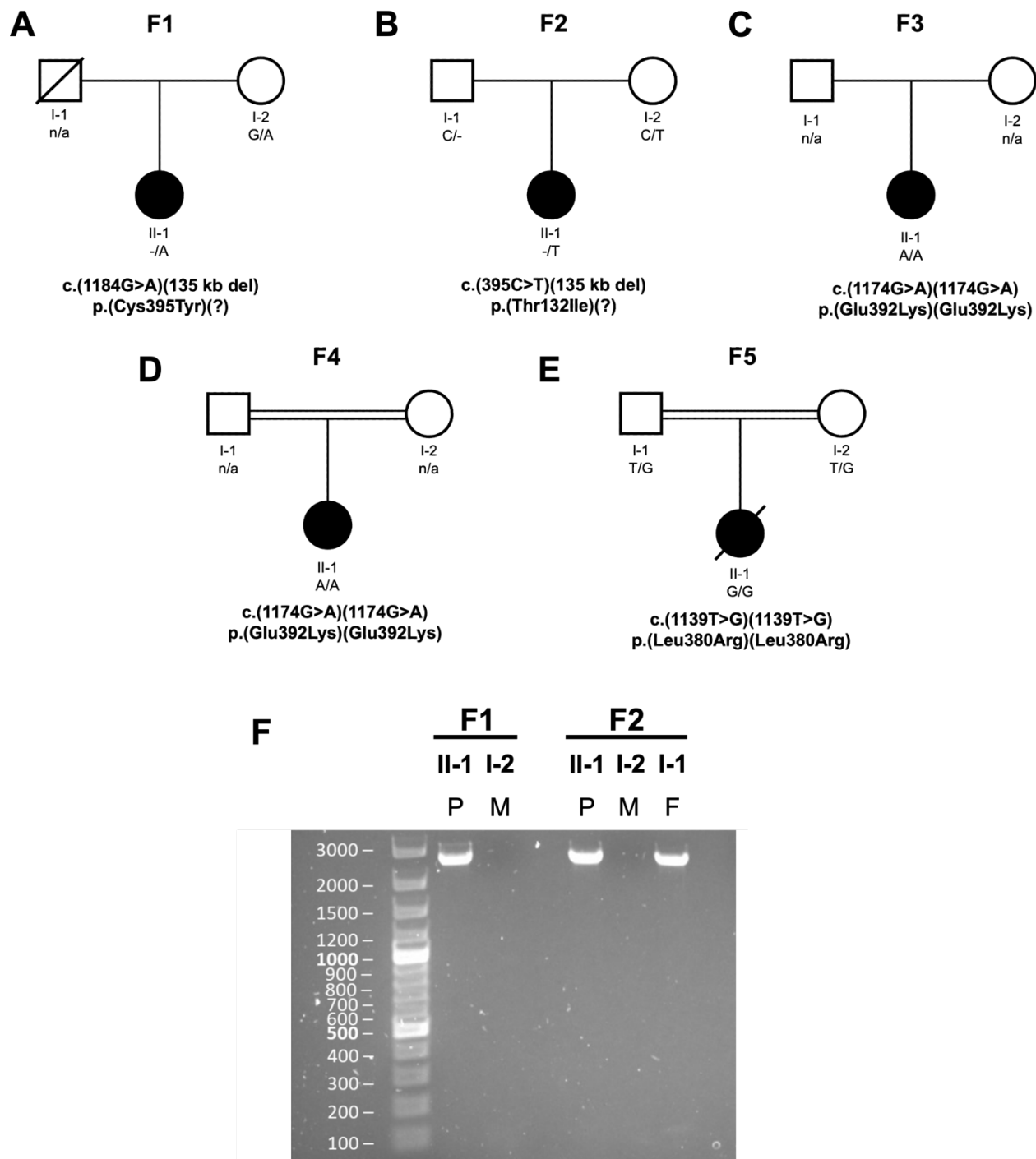
322

323 **Results**

324 Full phenotypic details are available from the authors on request.

325 Family F1 is a non-consanguineous white European family (Figure 1A) with an affected
326 female proband who was diagnosed with bilateral, profound SNHL in early childhood
327 (Figure S1A). She presented with primary amenorrhea leading to a diagnosis of Perrault
328 syndrome. Otherwise, she had normal development and intellect. She had a successful
329 unilateral cochlear implant as an adult. The mother is unaffected, whilst the father is
330 deceased from an unrelated condition.

331



332

333 **Figure 1: Family pedigrees and characterization of the *DAP3* deletion fusion product**
 334 **present in F1 and F2.**

335 (A-E) Pedigrees for the five families, with known segregation and variant details listed. All
 336 variants are annotated against the *DAP3* reference sequence NM_004632.4.

337 (F) PCR analysis of F1 and F2 DNA using gel electrophoresis to detect a fusion product
 338 for the 135 kb deletion. P = proband, M = mother, F = father.

339

340 WES initially uncovered no putative pathogenic variants in known Perrault syndrome
341 genes, but additional filtering revealed the F1 proband was compound heterozygous for
342 the missense variant *DAP3* (NM_004632.4:c.1184G>A, p.(Cys395Tyr)), *in trans* to a 135
343 kb deletion identified with multiplex ligation-dependent probe amplification (MPLA).
344 Breakpoints were established to recombine between Chr1(GRCh38):g.155641696-
345 155777755, which encompasses *DAP3* as well as *YY1AP1*, *GON4L* and *MSTO2P*. WES
346 data revealed no rare variants in these other genes. The *DAP3* variant p.(Cys395Tyr) was
347 confirmed as heterozygous in the unaffected mother by Sanger sequencing, however it is
348 unknown whether the deletion was a *de novo* event or inherited paternally.

349

350 Family F2 is a non-consanguineous white European family (Figure 1B), ascertained
351 through the Deciphering Developmental Disorders (DDD) study ²¹. The proband was
352 diagnosed with bilateral SNHL in early childhood. As an adult she had bilateral cochlear
353 implants (Figure S1B). She presented with primary amenorrhea (Figure S1C). In early
354 childhood, she experienced recurrent episodes of ketosis, lactic acidosis and
355 hypoglycemia and has mild intellectual disability. As an adult her brain MRI was normal.

356

357 Trio WES data in F2 identified a maternally inherited *DAP3* (NM_004632.4:c.395C>T
358 p.(Thr132Ile)) missense variant *in trans* to a paternally inherited 135 kb deletion. A PCR
359 fusion product of the same size as in the F1 proband was detected in the F2 proband, and
360 her unaffected father (Figure 1F). The repetitive nature of this chromosomal region made it
361 impossible to confirm whether the breakpoints are identical in both families.

	Proband F1	Proband F2	Proband F3	Proband F4	Proband F5
Sex	Female	Female	Female	Female	Female
Genotype (NM_004632.4)	c.1184G>A; 135 kb del	c.395C>T; 135 kb del	c.1174G>A; 1174G>A	c.1174G>A; 1174G>A	c.1139T>G; 1139T>G
Amino acid change (NP_001186778.1)	p.Cys395Tyr; ?	p.Thr132Ile; ?	p.Glu392Lys; Glu392Lys	p.Glu392Lys; Glu392Lys	p.Leu380Arg; Leu380Arg
Karyotype	46, XX	46, XX	N/A	N/A	N/A
Consanguinity	-	-	N/A	+	+
Bilateral sensorineural hearing loss	+	+	+	+	N/A
Severity	Profound	Profound	N/A	Profound	N/A
Treatment	Unilateral cochlear implant, previously bilateral hearing aids	Bilateral hearing aids; bilateral cochlear implants	N/A	Hearing aids	N/A
Primary ovarian insufficiency	+	+	+	N/A	N/A
Presentation	Primary amenorrhea	Primary amenorrhea	Primary amenorrhea	N/A	N/A
Lactic acidosis	-	+ (childhood)	N/A	+ (childhood)	+
Hypoglycemia	-	+ (childhood)	N/A	N/A	N/A

	Proband F1	Proband F2	Proband F3	Proband F4	Proband F5
Brain MRI	Normal	Normal	N/A	Diffuse leukoencephalopathy	Normal
Epilepsy	-	-	N/A	+	+
Intellectual disability	-	Mild	Mild	Severe	-
Renal dysfunction	-	-	-	Proximal tubulopathy	-
Retinopathy	-	-	-	+	-
Hepatomegaly	-	-	-	-	+
(Transient) liver failure	-	-	-	+	+
Height	148 cm	N/A	N/A	N/A	66 cm

363

364 Table 1: **Phenotypic summary of individuals with *DAP3* variants identified in this study.**

365 Blue – categories linked to SNHL, red – categories linked to POI. N/A = not available.

366

367

368

369 Family F3 was identified through Centogene. The proband is a young woman from Central
370 Asia (Figure 1C). She presented with bilateral SNHL of unknown severity, primary
371 amenorrhea, mild intellectual disability and developmental delay. No further clinical
372 information is available for this family. WES revealed the proband was homozygous for the
373 *DAP3* (NM_004632.4: c.1174G>A, p.(Glu392Lys)) missense variant.

374

375 Family F4 is a consanguineous family of North African ancestry (Figure 1D). The affected
376 proband is a girl who presented in early childhood with neurological impairment following a
377 febrile infection with seizures. Brain MRI revealed diffuse leukoencephalopathy, with a
378 lactate peak on spectroscopy (Figure S2). She had profound SNHL, transient liver failure
379 and proximal tubulopathy. Electroretinogram studies revealed retinopathy. CSF and blood
380 lactate levels were 4.5 mmol/L and 5-7 mmol/L respectively (normal ranges 1.1 – 2.4 and
381 ≤ 2 mmol/L), with an increased lactate/pyruvate ratio. Respiratory chain analysis activity
382 testing on muscle cells revealed a complex IV deficiency, with borderline complex I
383 deficiency. She has severe intellectual disability. The proband was homozygous for the
384 *DAP3* (NM_004632.4:c.1174G>A, p.(Glu392Lys)) missense variant.

385

386 Finally, family F5 is a consanguineous family from the Indian sub-continent with a family
387 history of neonatal and infant mortality (Figure 1E). The affected individual presented in
388 early childhood with fever, vomiting and lethargy. Further testing revealed
389 hepatosplenomegaly and lactic acidemia. Brain MRI was unremarkable. No hearing
390 evaluation was completed. The provisional diagnosis was mitochondrial disorder with
391 hepatic failure, and she died shortly after presentation. WES revealed the proband was
392 homozygous for the *DAP3* (NM_004632.4:c.1139T>G, p.(Leu380Arg)) missense variant.

393

394 All affected DAP3 residues are well-conserved; representing 65% (p.Thr132Ile), 91%
395 (p.Leu380Arg), 66% (p.Glu392Lys), and 73% (p.Cys395Tyr) of the respective amino acid
396 positions across 300 orthologs using ConSurf (Figure 2A). All substituted amino acids are
397 also not present in any orthologs ³⁰. Multiple *in silico* analyses predict these variants to be
398 pathogenic or deleterious (Table S6). The four missense variants are either absent or have
399 extremely low allele frequencies in the gnomAD v4.0 dataset (Table S7) ³¹, in further
400 support of pathogenicity.

401

408 reference sequence used for these species are listed accordingly: *H. sapiens*:
409 NP_001186778.1; *P. troglodytes*: XP_016802675.2; *C. familiaris*: XP_038527847.1; *B.*
410 *taurus*: NP_001106765.1; *R. norvegicus*: NP_001011950.2; *M. musculus*:
411 NP_001158005.1; *G. gallus*: XP_040546712.1; *X. tropicalis*: NP_001016002.1; *D. rerio*:
412 NP_001092207.1; *D. melanogaster*: NP_523811.1; *C. elegans*: AAD20727.1.

413 (B) Overview of *DAP3* variant locations, with additional regions or domains of interest for
414 additional context. MTS – mitochondrial targeting sequence, NR – nuclear receptor, CAYL
415 – cysteine alanine tyrosine leucine (final 4 residues at the *DAP3* C-terminus).

416 (C) Cryo-EM structure of human mitochondrial ribosome small subunit at 2.40 Å resolution
417 (PDB id: 7P2E), highlighting *DAP3* (green), *MRPS7* (rose) and *MRPS9* (yellow) subunits.

418 (D) Cartoon representation of *DAP3* bound with GDP and ADP.

419 (E) ADP binding site of *DAP3* in proximity to the four sites of mutation (orange sticks).

420

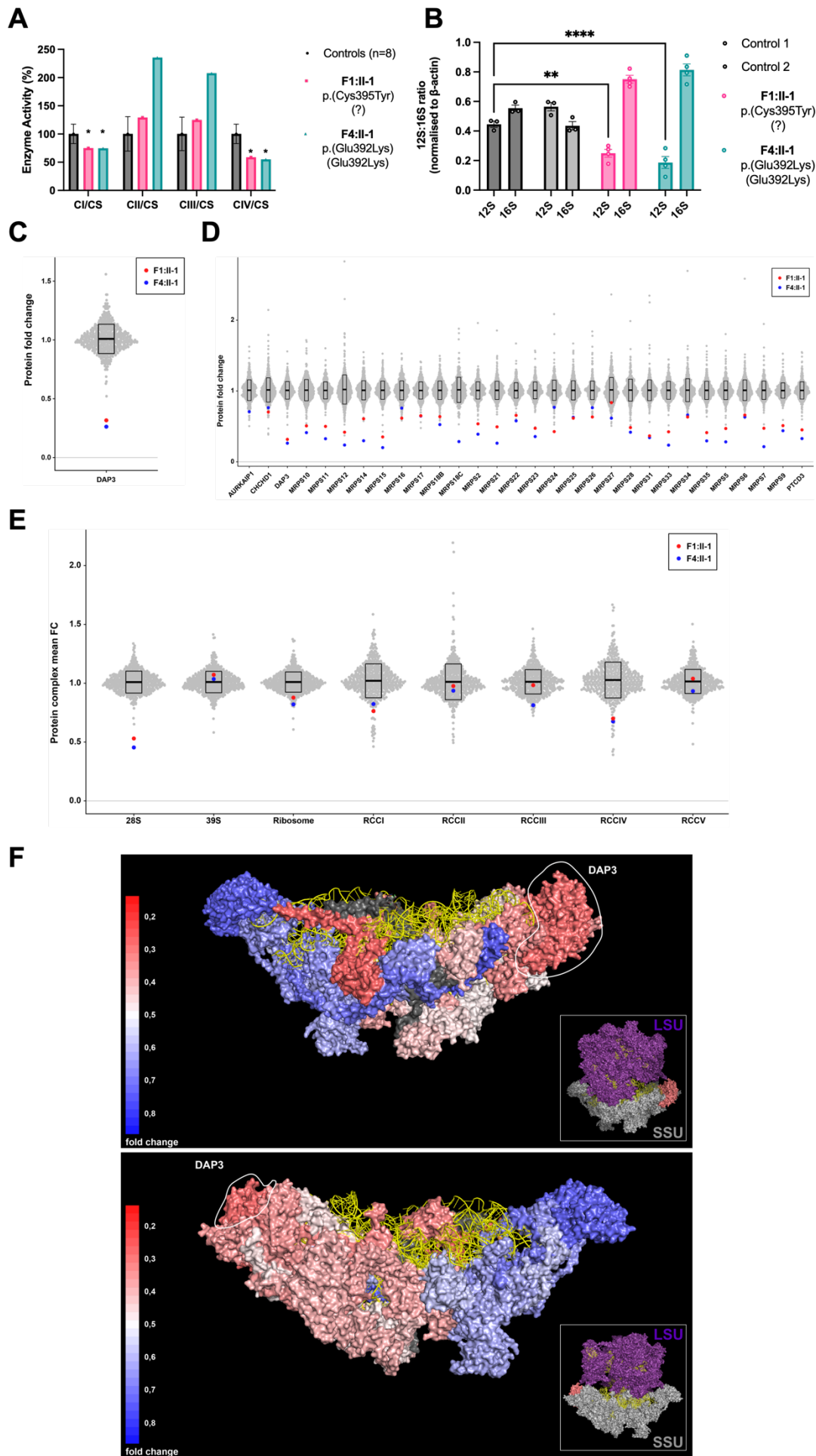
421 We next inspected the site of variants at the protein level (Figure 2B), based on the
422 recently determined structure of human mitoribosome SSU³³. *DAP3/MRPS29* is localized
423 in the head region of SSU (Figure 2C), close to the interface with the LSU. Three affected
424 residues sit around a nucleotide binding site, currently believed to bind ATP (Figure 2D).
425 Threonine 132 sits within a Walker A motif (**GEKGT**₁₃₂**GKT**), which is commonly
426 associated with ATP or GTP/GDP binding³⁴. Cysteine 395 is located within a putative
427 prenylation site (CAYL) at the *DAP3* C-terminus³⁵ and is close to the interface with
428 *MRPS7*, another mitoribosomal protein in which pathogenic variants have been associated
429 with primary ovarian insufficiency^{36,37} (Figure 2E). Glutamic acid 392 is located upstream
430 of this prenylation site and is predicted to interact directly with ATP³⁶. Leucine 380
431 localizes in an α -helix that packs against *MRPS7* and *MRPS9*.

432

433 To gain a deeper insight into the role of *DAP3* in the inner ear, we used

434 immunofluorescence to assess DAP3 localization within the mouse organ of Corti.
435 Endogenous DAP3 was identified within murine organ of Corti but was irregularly
436 distributed in hair cells before and after the onset of hearing, with higher expression
437 observed in likely damaged cells, sometimes with misshapen nuclei (Figure S3A).
438 Exogenous DAP3 tagged with EGFP was then transfected into the mouse organ of Corti
439 and vestibular sensory epithelium using a Helios gene gun, to test how overexpression
440 affected the inner ear sensory hair cells. Overexpression instigated co-localization of
441 DAP3-EGFP with TOM20 in hair cells and diffuse staining within the cell body (Figure
442 S3B), however, there was no discernible increase in cell death following DAP3
443 overexpression, indicating compensatory mechanisms may prevent unwarranted
444 alterations to mitochondrial and apoptotic functions in the inner ear. We also
445 immunostained transfected inner ear epithelial explants with DAP3 antibodies and showed
446 that antibody signal was increased in transfected cells only (Figure S3C), while remained
447 practically undetectable in non-transfected cells, indicating the specificity of the antibody to
448 DAP3 protein while pointing to very low levels of DAP3 in wild-type hair cells under normal
449 conditions.

450
451 To investigate the pathogenicity of the *DAP3* variants, we characterized dermal fibroblasts
452 obtained from the affected individuals in families F1 and F4. We assessed the respiratory
453 chain complex activities of these fibroblasts in comparison to eight healthy control
454 fibroblasts (Figure 3A). Interestingly, F1:II-1 proband fibroblasts exhibited a mild
455 mitochondrial respiratory chain defect, with a clear decline in complex IV activity compared
456 to control reference ranges. F4:II-1 fibroblasts exhibited a heightened respiratory chain
457 defect, with a reduction in both complex I and complex IV activities (Tables S8-9). The F4
458 CI:CII ratio of activities was also decreased, indicative of a generalized disorder of
459 mitochondrial translation.



461 **Figure 3: Functional and proteomic analysis of F1 and F4 proband fibroblasts reveal**
462 ***DAP3* variants induce mitochondrial respiratory chain defects and decreased**
463 **expression levels of small mitoribosomal subunit and OXPHOS components.**

464 (A) Mitochondrial respiratory chain enzyme activities in control (black), F1:II-1 (pink) and
465 F4:II-1 (blue) fibroblast samples. Mean enzyme activities in control fibroblasts (n = 8) are
466 set at 100%. Error bars represent standard deviation between the controls.

467 * indicates enzyme activity is beyond control standard deviation values.

468 (B) *MT-RNR1* (12S) and *MT-RNR2* (16S) expression levels in fibroblast cDNA. Data
469 expressed as a ratio using relative quantification (RQ) values. Error bars represent the
470 SEM. N = 3-4, **p < 0.01, ****p < 0.0001, two-way ANOVA with Tukey's multiple
471 comparisons test, comparing 12S RQ value of controls to affected individuals.

472 (C) *DAP3* protein levels in affected individual fibroblasts expressed as protein fold change
473 compared to the mean of 512 fibroblast samples.

474 (D) Protein fold change of all components of the mitoribosomal SSU in affected individual
475 fibroblasts, compared to 512 controls.

476 (E) Grouped mean fold change of all proteins comprising mitoribosome subunits, whole
477 mitoribosome, and OXPHOS components compared to the mean values of 512 controls.

478 (F) Cryo-EM structure (PDB id: 6VLZ) of mitoribosomal SSU with individual subunits
479 colored according to their mean fold change values (of individuals F1:II-1 and F4:II-1)
480 compared to the mean of 512 controls. Colors ranging from weakly reduced (blue) to
481 strongly reduced (red) and two subunits (MRPS18C and MRPS38) in dark grey as no
482 mean fold change values could be calculated. 12S ribosomal RNA is colored in yellow,
483 *DAP3* is marked by a circle, and the small inset shows the relative position within the 55S
484 ribosome.

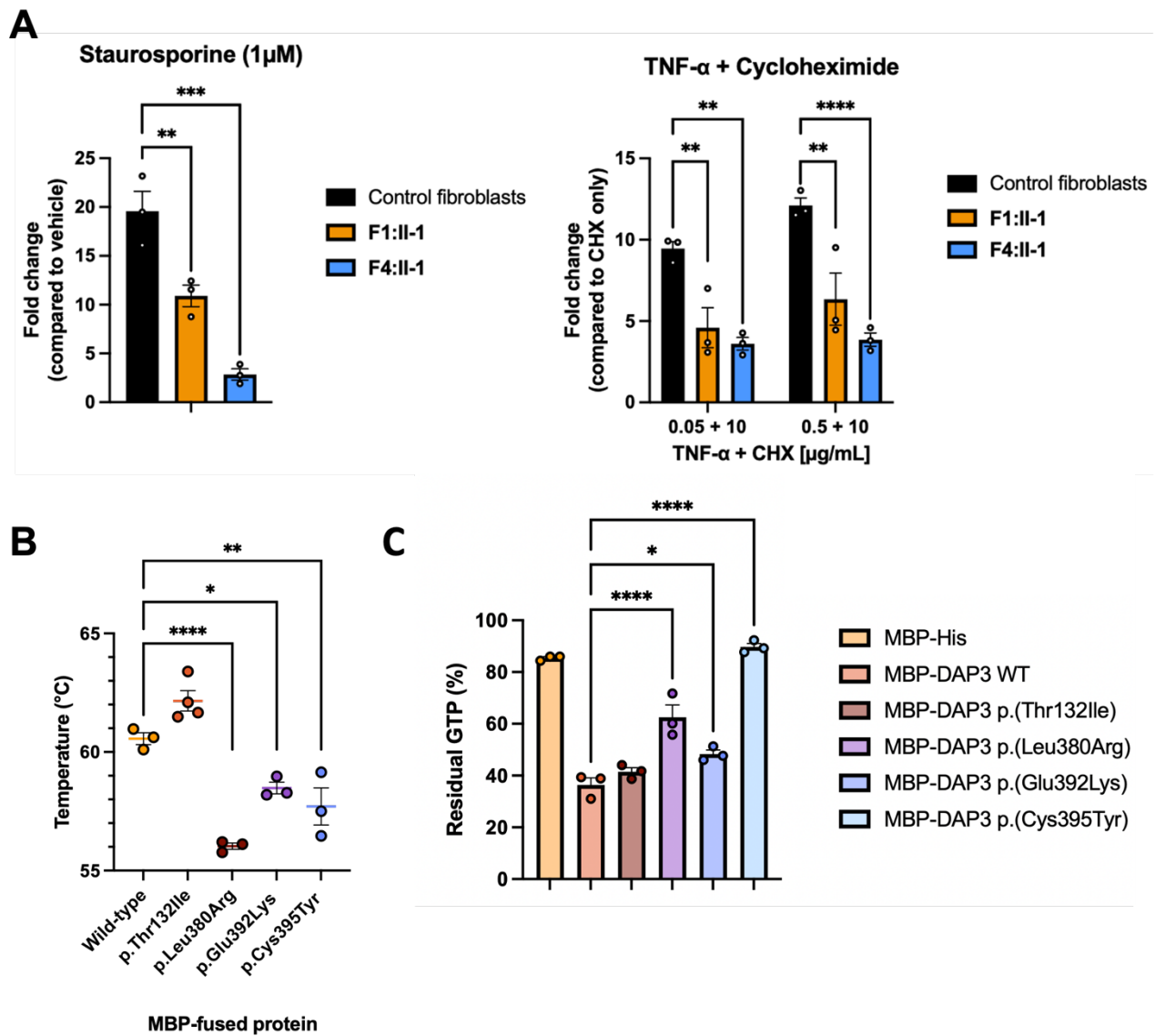
485

486 As *DAP3* is a component of the small mitoribosomal subunit, we assessed if expression of

487 *MT-RNR1* and *MT-RNR2*, which encode 12S and 16S rRNA respectively, was altered in
488 F1:II-1 and F4:II-1 fibroblasts compared to healthy controls. The subsequent 12S:16S
489 ratios were calculated using *MT-RNR1* and *MT-RNR2* relative quantification values to
490 highlight specific contextual alterations to the small mitoribosomal subunit. The 12S
491 component of the 12S:16S ratio was significantly reduced in F1:II-1 and F4:II-1 cDNA
492 compared to controls, with the DAP3 p.Glu392Lys variant producing the strongest effect
493 on *MT-RNR1* expression ($p = <0.0001$ (p.Glu392Lys;Glu392Lys) and 0.0019
494 (p.Cys395Tyr;?)) (Figure 3B). These data indicate an impairment of mitoribosomal
495 assembly.

496
497 To assess whether *DAP3* variants influence levels of DAP3, mitoribosomal subunits, or
498 other mitochondrial proteins, fibroblasts from F1:II-1 and F4:II-1 underwent proteomic
499 analysis. The data were compared to a cohort of 512 individuals to visualize outliers.
500 Interestingly, DAP3 was reduced to approximately 25% of mean levels in fibroblasts from
501 both affected individuals, whilst also displaying the lowest DAP3 levels compared to any
502 other individual in the dataset (Figure 3C). There was a remarkably consistent decrease in
503 levels across all proteins constituting the small mitoribosomal subunit complex (Figure 3D)
504 in fibroblasts from both affected individuals compared to the cohort, unless the protein was
505 undetected in the mass spectrometry analysis (Table S10). When summing up the SSU
506 and LSU overall, the two individuals with *DAP3* variants show the lowest SSU levels
507 across the full cohort of samples, whilst the levels of LSU were not affected (Figure 3E).
508 The analysis of mitochondrial respiratory chain complexes revealed a reduction of complex
509 I and complex IV subunits in both affected individuals. Moreover, F4:II-1 also displayed a
510 reduction in complex III. This reduction agrees with the enzymatic analysis and reflect the
511 downstream consequences on the translation of mtDNA-encoded respiratory chain
512 complex subunits. To visualize subunit protein abundance in the context of its 3D

513 structure, the data were mapped onto the Cryo-EM structure of the SSU (Figure 3F).
514 Generally, proteins situated near DAP3 in the SSU are less abundant, with subcomplex
515 formation more likely if situated on the opposite side to DAP3. These findings demonstrate
516 independent evidence that *DAP3* variants impair assembly of the mitoribosomal SSU,
517 impacting mitochondrial translation.
518
519 To assess whether disease-associated variants affect apoptosis, we cultured fibroblasts
520 from F1:II-1 and F4:II-1 and challenged them with common effectors of intrinsic and
521 extrinsic apoptosis pathways. We measured caspase-3 and caspase-7 activities with a
522 commercial luminescence-based assay. Treatment with both staurosporine and TNF- α +
523 cycloheximide significantly reduced caspase-3/7 release in affected individual fibroblasts
524 compared to controls (Figure 4A). The fibroblasts from F4:II-1 exhibited a stronger
525 apoptotic defect when challenged with intrinsic stimuli compared to the fibroblasts from
526 F1:II-1. However, there were no significant differences between fibroblasts from affected
527 individuals when treated with extrinsic stimuli.



528

529 **Figure 4: Functional analysis of both affected individual fibroblasts and**
 530 **recombinant DAP3 protein establish *DAP3* variants can diminish apoptotic**
 531 **sensitivity and destabilize *DAP3* protein structure, impacting GTPase activity.**

532 (A) Assessment of caspase-3/7 release following stimulation of intrinsic and extrinsic
 533 apoptotic pathways. Affected individual fibroblasts were challenged in duplicate with
 534 staurosporine for 4.5 hours, or TNF- α + cycloheximide (CHX) for 24 hours before addition
 535 of assay reagent. Data expressed as fold change in luminescence signal compared to
 536 DMSO-treated or CHX-treated fibroblasts, with error bars representing SEM. N = 3, **p <
 537 0.01, ***p < 0.001, ****p < 0.0001, using one-way ANOVA with Dunnett's multiple
 538 comparisons test (staurosporine) or two-way ANOVA with Dunnett's multiple comparisons

539 test (TNF- α), comparing affected individual fibroblasts to control.

540 (B) Thermal stability of recombinant wild-type and variant MBP-DAP3 protein. Data points
541 represent average T_m of triplicate reactions. Error bars represent SEM. N = 3-4, * $p < 0.05$,
542 ** $p < 0.01$, **** $p < 0.0001$, using one-way ANOVA with Dunnett's multiple comparisons
543 test, comparing wild-type to variants.

544 (C) GTPase activity of recombinant wild-type and variant MBP-DAP3 protein. Data
545 presented as mean luminescence produced by residual GTP, with error bars representing
546 SEM. N = 3, * $p < 0.05$, **** $p < 0.0001$, one-way ANOVA with Dunnett's multiple
547 comparisons test, comparing wild-type protein activity to variants.

548 To investigate the effect of *DAP3* variants on protein stability, we generated recombinant
549 wild-type and variant *DAP3* fused to maltose-binding protein (MBP). Thermal shift assay
550 (TSA) and subsequent melt-curve analysis highlighted a significant T_m decrease in
551 p.Leu380Arg, p.Glu392Lys and p.Cys395Tyr protein compared to wild-type (Figure 4B),
552 indicating unfolding at lower temperatures and consequently reduced stability. Proteomic
553 dissection of mitoribosomes indicated that *DAP3* is the only GTP-binding protein in the
554 SSU, suggesting that it could initiate or play a key role in mitochondrial protein synthesis
555 ^{10,38}. We hypothesized that *DAP3* variants could impair intrinsic GTPase activity, as
556 disease-associated variants can impair *DAP3* stability. Firstly, wild-type MBP-*DAP3*
557 exhibited GTPase activity *in vitro*. This GTPase activity was found to be significantly
558 reduced with the *DAP3* p.Leu380Arg, p.Glu392Lys and p.Cys395Tyr variant protein ($p =$
559 <0.0001 , 0.0206 and <0.0001 respectively), correlating with the TSA data (Figure 4C). The
560 impact of these variants was variable, with a modest increase in residual GTP observed
561 with p.Glu392Lys compared to wild-type. However, the p.Cys395Tyr variant increased
562 residual GTP to the level observed with the negative control MBP-His, indicating low
563 GTPase activity. Interestingly, there was no significant change in GTPase activity or
564 thermal stability with p.Thr132Ile variant protein. These data suggest *DAP3* variants can

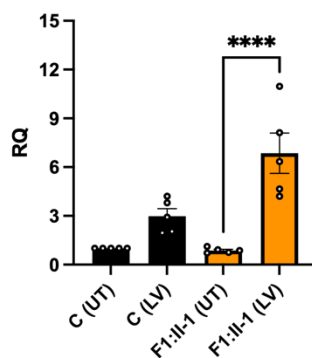
565 reduce protein stability, subsequently impairing ligand binding and GTPase activity.

566

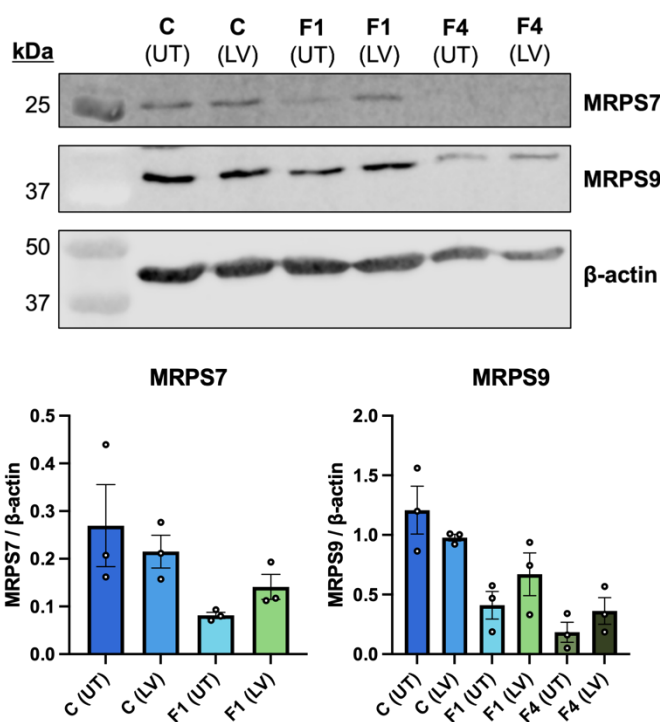
567 To further confirm *DAP3* variant pathogenicity and specificity of their effect, we transduced
568 fibroblasts from F1:II-1 and F4:II-1 with a lentiviral vector expressing wild-type *DAP3* to
569 assess whether the mitoribosomal deficit could be rescued. *DAP3* mRNA expression
570 increased in transduced cells, as expected (Figure 5A). Basal MRPS7 and MRPS9 levels
571 were reduced in affected individuals, concordant with proteomic analysis. Following
572 lentiviral transduction, immunoblotting also revealed a partial rescue of MRPS7 and
573 MRPS9 protein levels in affected individual fibroblasts (Figure 5B), as well as in
574 components of respiratory chain complex I (NDUFB8) and IV (COX II) (Figure 5C),
575 changes which were not observed in transduced control fibroblasts.

A

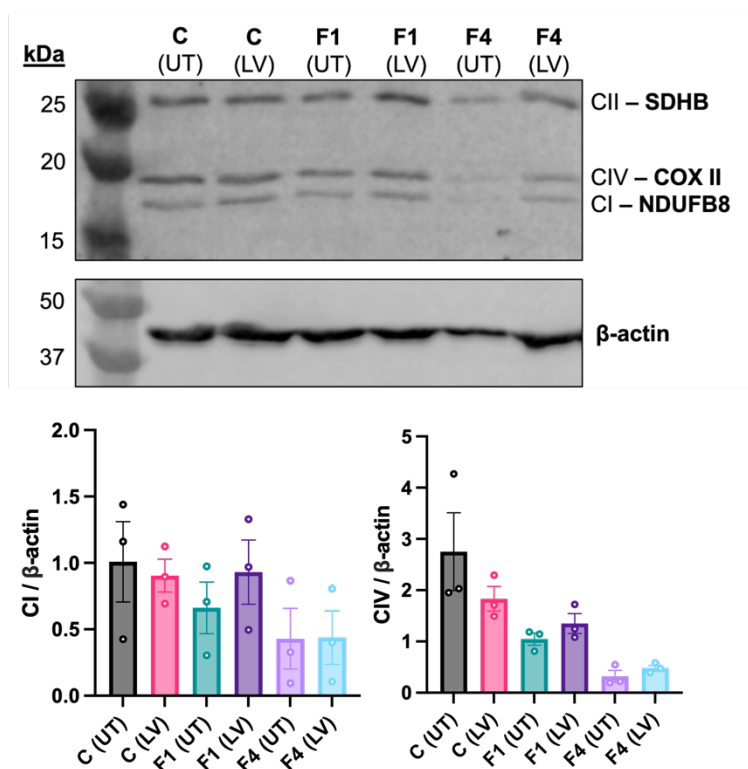
DAP3 mRNA expression



B



C



577 **Figure 5: Lentiviral transduction of wild-type *DAP3* increases protein levels of**
578 **MRPS7, MRPS9 and OXPHOS components in F1:II-1 and F4:II-1 fibroblasts.**

579 (A) Expression of *DAP3* mRNA in control and fibroblasts from F1:II-1 after lentiviral
580 transduction (LV) of *DAP3* cDNA for 72 hours, or untransduced (UT). Each datapoint
581 represents an averaged RQ value from triplicate reactions, using cDNA from independent
582 transductions. Error bars represent SEM. N = 5, ****p < 0.0001, one-way ANOVA with
583 Tukey's multiple comparisons test.

584 (B) Protein levels of MRPS7 and MRPS9 in control fibroblasts and fibroblasts from F1:II-1
585 and F4:II-1 after lentiviral transduction of *DAP3* cDNA for 72 hours. Beta-actin was used
586 as a loading control and for densitometric analysis. Blots are representative of results from
587 3 independent biological repeats. MRPS7 levels were unable to be quantified in fibroblasts
588 from F4:II-1.

589 (C) Protein levels of SDHB, COX II and NDUFB8 in control fibroblasts and fibroblasts from
590 F1:II-1 and F4:II-1 after lentiviral transduction of *DAP3* cDNA for 72 hours. Blots are
591 representative of results from 3 independent biological repeats.

592

593 **Discussion**

594 Using a range of genetic, molecular and proteomic techniques, this study reveals that
595 biallelic *DAP3* variants are associated with a Perrault syndrome-spectrum phenotype.
596 Most known Perrault syndrome-associated genes encode mitochondrial proteins with key
597 roles in mitochondrial translation, which is consistent with *DAP3* being a mitoribosomal
598 SSU protein.

599 Phenotypes of individuals with *DAP3* disease-associated variants include a variety of
600 features consistent with mitochondrial dysfunction, including lactic acidemia, neurological
601 dysfunction, SNHL and POI, with variable expression (Table 1). Phenotypic severity
602 ranges from classic Perrault syndrome, extending to childhood-onset neurological,

603 developmental and multisystem abnormalities. The affected individuals homozygous for
604 the same missense variant p.(Glu392Lys) have markedly different phenotypic
605 presentations, with F4:II-1 affected with neurological, renal and retinal presentations. The
606 probands from F1 and F2 have phenotypes which are less severe than in family F4. Both
607 individuals from F1 and F2 have a hemizygous *DAP3* missense variant *in trans* to a 135 kb
608 deletion, consistent with complete loss of function of one allele.

609
610 Diminished respiratory chain complex activities in fibroblasts from two affected individuals
611 are consistent with a mitochondrial translation deficit (Figure 3A). Interestingly, the
612 fibroblasts from F4:II-1 exhibited a more pronounced respiratory chain defect, with a clear
613 reduction in both complex I and IV activities and diminished complex I:II ratios indicating a
614 generalized disorder of mitochondrial translation. These data highlight that distinct *DAP3*
615 variants have variable impacts on mitochondrial function.

616
617 The mtDNA-encoded 12S and 16S rRNA are essential components of the mitoribosomal
618 SSU and LSU, respectively. They enable protein-RNA and protein-protein interactions
619 which are key requirements for mitoribosome assembly and integrity³⁹. 12S:16S mRNA
620 ratios have previously been evaluated to highlight specific discrepancies in mt-rRNA levels
621⁴⁰. 12S rRNA is associated with Perrault syndrome due to disease-associated variants in
622 the rRNA chaperone ERAL1, which also interacts with *DAP3*^{40,41}. *DAP3* is closely
623 associated with the 12S rRNA, and when individual MRPS are diminished, 12S rRNA
624 levels decline leading to SSU assembly defects¹⁷. We hypothesized that 12S rRNA levels
625 could be reduced in fibroblasts from affected individuals as *DAP3* is assembled into the
626 SSU at an early stage⁵, and disrupted *DAP3* function could lead to reduced mitoribosomal
627 assembly and integrity. Indeed, 12S rRNA levels were significantly decreased in
628 fibroblasts, whilst 16S rRNA levels were unchanged (Figure 3B).

629

630 Using sensitive quantitative proteomic profiling, biallelic *DAP3* variants were observed to
631 confer a profile of mitochondrial ribosomal proteins typical for a SSU deficiency. Both
632 fibroblasts from affected individuals demonstrated a clear, specific reduction in the levels
633 of *DAP3*, but also all other SSU proteins, with all LSU proteins unaffected (Figure 3C-E).
634 These data indicate that *DAP3* variants result in a specific impairment of SSU assembly.
635 The loss of *DAP3* could result in failure to assemble the mitoribosomal SSU triggering
636 degradation of the 12S rRNA and other MRPs that require *DAP3* or 12S rRNA as an
637 assembly scaffold. The generalized decrease in SSU protein levels was more evident in
638 fibroblasts from F4:II-1, consistent with her phenotypic severity. Proteomic profiles
639 revealed the functional consequence of impaired assembly of mitoribosome as reduced
640 mitochondrial translation of mtDNA encoded subunits of the respiratory chain complexes.
641 Multiple respiratory chain complex proteins were reduced. Mainly complex I and IV mean
642 protein abundance was affected in fibroblasts of both affected individuals, although
643 complex III abundance was also reduced in F4:II-1, reflecting a more apparent generalized
644 respiratory chain complex defect in this individual. The reduced respiratory chain complex
645 activity of complex I and IV is consistent with other monogenic mitochondrial disorders
646 ^{42,43}, and variants in other MRPs, including *MRPS2*, *MRPS34* and *MRPL24* which result in
647 impaired mitoribosome assembly ⁴⁴⁻⁴⁶. However, despite the common molecular effects,
648 the clinical presentation of individuals with biallelic pathogenic variants in mitoribosomal
649 proteins is heterogenous.

650

651 Interestingly, in the fibroblasts from F4:II-1, the largest reduction was observed in *MRPS7*
652 levels. Variants in *MRPS7* have been associated with clinical features overlapping Perrault
653 syndrome ^{17,37}. *DAP3* and *MRPS7* are predicted to interact extensively, including at
654 Cys395 ³⁶, which may explain the shared phenotypic spectrum. Variants in the gene

655 encoding 12S rRNA are associated with sensorineural, non-syndromic deafness ⁴⁷,
656 suggesting altered MRPS7 and 12S rRNA interactions due to their reduced abundance
657 may account for the SNHL in individuals with variants in *DAP3*.

658
659 We mapped protein mean fold change values seen with *DAP3* variants onto a Cryo-EM
660 structure of the SSU to visualise SSU protein abundance within a structural context (Figure
661 3F). Interestingly, subunit abundance does not always reflect its proximity to *DAP3*. For
662 example, MRPS12 and MRPS15 levels were substantially decreased in both sets of
663 fibroblasts. Both MRPS12 and MRPS15 are assemble late to the SSU and are distant from
664 *DAP3*, yet both interact extensively with 12S rRNA ^{5,48}, which may reflect the importance
665 of steady-state 12S levels for successful assembly and stability.

666
667 Intriguingly, four SSU proteins (MRPS7, MRPS12, MRPS15, MRPS33) exhibited marked
668 depletion, especially in fibroblasts from F4:II-1. The 392 residue is predicted to interact
669 with ATP, a ligand which stabilizes *DAP3*, and two neighboring residues Ser389 and
670 Arg393 also contact an unpaired base of the 12S rRNA which may also stabilize the
671 mitoribosome ⁴⁹. This observation may indicate the *DAP3* p.(Glu392Lys) variant is more
672 likely to induce structural defects that impair initial sub-complex assembly, and reduction in
673 SSU proteins in this individual. Taken together, these data demonstrate *DAP3* variants
674 effect a global reduction in SSU protein levels leading to impaired mitoribosome assembly
675 and mitochondrial translation.

676
677 Previous data has suggested multiple Perrault syndrome-associated genes are distinctly
678 expressed within the spiral ganglion neurons of the cochlea, predicting variants could
679 interfere with auditory signal transmission ¹³. Mouse organ of Corti immunostaining did not
680 suggest any obvious *DAP3* localization patterns to specific compartments of the inner ear

681 (Figure S3A), in contrast to Perrault syndrome associated PRORP which was localized to
682 synapses and nerve fibers of hair cells⁵⁰. Diffuse DAP3 cytoplasmic staining partially
683 overlapping with mitochondrial marker TOM20 staining was observed before and after the
684 onset of hearing in wild-type mice in some hair cells which sometimes appeared damaged
685 with misshapen nuclei (Figure S3A). Exogenous overexpression shows increased
686 mitochondrial localization in hair cells without cell damage (Figure S3B-C). These data
687 imply DAP3 is present within the mouse inner ear at relatively low levels with no clear
688 localization profile but might be upregulated in some stress conditions, indicating that
689 SNHL in individuals with Perrault syndrome may have diverse gene specific etiologies.

690
691 Treating fibroblasts from affected individuals with intrinsic and extrinsic apoptosis
692 mediators revealed a decrease in apoptotic sensitivity compared to controls (Figure 4A).
693 These data contrast with previous studies evaluating the role of DAP3 in apoptosis, which
694 have described variable effects on extrinsic receptor-mediated cell death but no
695 desensitizing effects reported via the intrinsic mitochondrial-mediated death mechanism
696^{10,51}. It is possible that DAP3 disease-associated variants or the subsequent reduction in
697 DAP3 abundance could affect interactions with known mediators of the intrinsic apoptosis
698 pathway, or cells damaged by impaired mitoribosome assembly could induce non-specific
699 mechanisms that impair the ability of the cell to detect or stimulate components of the
700 intrinsic apoptosis pathway. DAP3 has been proposed to act as an adapter protein for
701 death-inducing signaling complexes involved in the extrinsic pathway, recruiting FADD to
702 TRAIL receptors (DR4 and DR5) in a GTP-dependent manner which may be aided by
703 DAP3-binding protein death ligand signal enhancer (DELE1)^{52,53}. Diminished and
704 unstable DAP3 protein can lead to reduced death receptor assembly, and subsequent
705 signal transduction could explain the reduced sensitivity of fibroblasts from affected
706 individuals to TNF- α .

707

708 Melt-curve analysis revealed *DAP3* variants p.Leu380Arg, p.Glu392Lys and p.Cys395Tyr
709 exhibited significantly lower melting temperatures than wild-type, demonstrating these C-
710 terminal variants destabilize *DAP3* (Figure 4B). These data broadly correlate with the
711 GTPase results, indicating the decreased stability could impair ligand binding and
712 indirectly interfere with subcomplex assembly and mitochondrial protein synthesis. The
713 *DAP3* p.Leu380Arg variant conferred the most severe effect on thermal stability,
714 consistent with the severe clinical phenotype. The p.Thr132Ile variant had no effect on
715 thermal stability, so how this variant results in disease remains undetermined. However,
716 residue 132 sits within the highly conserved Walker A motif [GxxxxGK(S/T)] which is
717 necessary for ATP binding ³⁴.

718

719 Proteins with GTPase activity can act as molecular switches and regulate a series of cell
720 signaling events, including mitoribosome assembly. Mitoribosome assembly GTPases,
721 such as ERAL1 and GTP-binding protein 10 (GTPBP10), can participate as rRNA
722 chaperones and assembly factors, as well as conducting rRNA modifications and subunit
723 quality control ^{54,55}. *DAP3* is the only predicted GTPase of the mitoribosome ³⁸, but the
724 functional extent of its putative GTPase activity is unclear. A recent structural study
725 suggested that *DAP3* GTPase activity is independent of the translation cycle of the
726 mitoribosome. However, GDP binding to *DAP3* was predicted to be required for efficient
727 mitochondrial protein synthesis via enhanced stability of the *DAP3* β -hairpin at residues
728 208-216 ⁴⁹, highlighting the importance of *DAP3* GDP binding to global mitoribosome
729 function. We sought to understand if recombinant *DAP3* exhibited intrinsic GTPase
730 activity, and if GTPase activity was affected by the disease-associated variants. *DAP3*
731 variants p.Leu380Arg, p.Glu392Lys and p.Cys395Tyr significantly reduced GTPase
732 activity, but *DAP3* p.Thr132Ile had no effect (Figure 4C). These *DAP3* residues are not

733 located close to the GDP binding region, which suggested reduced stability and improper
734 folding may non-specifically destabilize the GDP binding pocket. Residual GTPase activity
735 does not appear to correlate with phenotype severity, as the individual who is compound
736 heterozygous for p.Cys395Tyr has the least severe clinical presentation. Specific variants
737 such as DAP3 p.Cys395Tyr may also alter key DAP3 modifications such as farnesylation
738 of the CAYL motif³⁵. However, it is unclear if DAP3 is sufficiently prenylated *in vivo* for this
739 modification to contribute to phenotypic variability³⁸.

740

741 Rescue experiments were performed to further verify *DAP3* variant pathogenicity.
742 Lentiviral transduction of wild-type *DAP3* increased *DAP3* mRNA expression (Figure 5A).
743 Immunoblotting revealed transduction increased MRPS7 levels in fibroblasts from F1:II-1,
744 and MRPS9 levels in fibroblasts from F1:II-1 and F4:II-1 compared to untransduced cells,
745 but not to control fibroblast protein levels (Figure 5B). This trend was not observed in
746 control fibroblasts. The levels of CI and CIV subunits, NDUFB8 and COXII, respectively
747 were also partially rescued in transduced fibroblasts, particularly in F1:II-1 fibroblasts
748 (Figure 5C). This indicates that a partial rescue of depleted mitoribosomal SSU proteins in
749 affected individual fibroblasts may aid stability of the mitoribosomal SSU, thus partially
750 restoring CI and CIV biogenesis. This effect has been observed in several functional
751 studies confirming variant pathogenicity in other SSU-encoding genes, further confirming
752 that mitoribosome destabilization is associated with various heterogenous mitochondrial
753 disorders^{45,46,56,57}. Collectively, these data indicate biallelic *DAP3* variants result in a
754 Perrault syndrome spectrum phenotype, destabilizing the mitoribosome and impairment of
755 mitochondrial translation.

756 Applying the ClinGen scoring criteria for gene-disease validity, we calculated a disease
757 association score of 11 consistent with moderate evidence for disease association, which
758 cannot be strengthened further without identification and characterization of additional

759 affected individuals⁵⁸. However, the combined genetic, clinical and functional evidence
760 outlined in this study provide confidence that biallelic *DAP3* variants are responsible for
761 the described clinical presentations.

762

763 In summary, we have identified five independent families with biallelic variants in *DAP3*
764 with a pleiotropic Perrault syndrome-associated phenotype, expanding the genetic
765 heterogeneity of Perrault syndrome and further emphasizing the importance of
766 mitochondrial translation in health and disease.

767

768

769

770

771

772 **Acknowledgements**

773 We thank the families for their participation. This study was supported by the Medical
774 Research Council (MR/W019027/1 ROK, RWT and WGN), Action on Hearing Loss (S35
775 Newman); Royal National Institute for the Deaf and Masonic Charitable Foundation
776 (S60_Newman); Action Medical Research (GN2494); NIHR Manchester Biomedical
777 Research Centre ((IS-BRC-1215-20007 and NIHR203308); Infertility Research Trust;
778 Wellcome Trust ISSF pump-prime award [097820/Z/11/B]; the Wellcome Trust Centre for
779 Mitochondrial Research (203105/Z/16/Z to RWT); the UK NHS Highly Specialised “Rare
780 Mitochondrial Disorders of Adults and Children” Service (RWT); and The Lily Foundation
781 (RWT) through PhD studentship funding to RICG; DBT/Wellcome Trust India Alliance for
782 the study, “Centre for Rare Disease Diagnosis, Research and Training”
783 (IA/CRC/20/1/600002); in part by the Intramural Research Program of the NIDCD at the
784 NIH (DC000039 to TBF). The DDD study presents independent research commissioned
785 by the Health Innovation Challenge Fund [grant number HICF-1009-003], a parallel
786 funding partnership between Wellcome and the Department of Health, and the Wellcome
787 Sanger Institute [grant number WT098051]. The research team acknowledges the support
788 of the National Institute for Health Research, through the Comprehensive Clinical
789 Research Network. The views expressed in the paper are those of the authors and not
790 necessarily those of the funders.

791 **Ethical approval**

792 All individuals or their guardians provided written informed consent in accordance with
793 local regulations. Ethical approval for this study was granted by the National Health
794 Service Ethics Committee (16/WA/0017) and University of Manchester. The NIH Animal
795 Use Committee approved protocol 1263-15 to T.B.F. for murine studies.

796

797 **Author Contributions**

798 TS, RK, LAMD, AS, HBT, CB, KT, MO, RICG, EMJ, AJ, IAB, MB, JEU, JOS, SGW, SSB,
799 AJB, SC, JME generated laboratory data. MS, SJ, GSC, AS, MY, PR, HA, ABC, MEB, HH
800 and WGN contributed genetic and clinical data. TBS, RK, LAMD, CB, SB, WWY, KM, TBF,
801 RWT, HP, ROK and WGN designed and supervised the experiments and analyzed the
802 data. TBS, ROK, WGN drafted the paper. All authors reviewed and critically contributed to
803 the paper.

804

805 **Declaration of interest**

806 The authors declare no competing interests.

807

808 **Web Resources**

809 dbSNP, <https://www.ncbi.nlm.nih.gov/projects/SNP/>

810 Ensembl Variant Effect Predictor (VEP),

811 <https://www.ensembl.org/info/docs/tools/vep/index.html>

812 Exome Variant Server, <http://evs.gs.washington.edu/EVS/>

813 GenBank. <https://www.ncbi.nlm.nih.gov/genbank/>

814 GeneMatcher, <https://genematcher.org/>

815 GTEEx, <https://gtexportal.org/home/>

816 gnomAD, <http://gnomad.broadinstitute.org/>

817 FoldX, <http://foldxsuite.crg.eu/>

818 LOVD, <https://www.lovd.nl/>

819 OMIM, <https://www.omim.org/>

820 MutationTaster, <http://www.mutationtaster.org/>

821 PolyPhen-2, <http://genetics.bwh.harvard.edu/pph2/>

822 SIFT, <http://sift.bii.a-star.edu.sg>

823

824 **Data and code availability**

825 The *DAP3* variants were submitted to ClinVar (<https://www.ncbi.nlm.nih.gov/clinvar/>)
826 (GenBank: NM_004632.4; accession numbers SCV004228990 – SCV004228993,
827 VCV003066057.1).

828

829 **References**

- 830 1. Amunts A, Brown A, Toots J, Scheres SHW, Ramakrishnan V. The structure of the
831 human mitochondrial ribosome. *Science*. 2015;348(6230):95-98.
832 doi:10.1126/science.aaa1193
- 833 2. Greber BJ, Bieri P, Leibundgut M, Leitner A, Aebersold R, Boehringer D, Ban N.
834 Ribosome. The complete structure of the 55S mammalian mitochondrial ribosome.
835 *Science*. 2015;348(6232):303-308. doi:10.1126/science.aaa3872
- 836 3. Itoh Y, Andréll J, Choi A, Richter U, Maiti P, Best RB, Barrientos A, Battersby BJ,
837 Amunts A. Mechanism of membrane-tethered mitochondrial protein synthesis.
838 *Science*. 2021;371(6531):846-849. doi:10.1126/science.abe0763
- 839 4. Kummer E, Leibundgut M, Rackham O, Lee RG, Boehringer D, Filipovska A, Ban N.
840 Unique features of mammalian mitochondrial translation initiation revealed by cryo-EM.
841 *Nature*. 2018;560(7717):263-267. doi:10.1038/s41586-018-0373-y
- 842 5. Bogenhagen DF, Ostermeyer-Fay AG, Haley JD, Garcia-Diaz M. Kinetics and
843 Mechanism of Mammalian Mitochondrial Ribosome Assembly. *Cell Rep*.
844 2018;22(7):1935-1944. doi:10.1016/j.celrep.2018.01.066
- 845 6. Lopez Sanchez MIG, Krüger A, Shiriaev DI, Liu Y, Rorbach J. Human Mitoribosome
846 Biogenesis and Its Emerging Links to Disease. *International Journal of Molecular*
847 *Sciences*. 2021;22(8):3827. doi:10.3390/ijms22083827

- 848 7. Tang T, Zheng B, Chen S hong, Murphy AN, Kudlicka K, Zhou H, Farquhar MG.
849 hNOA1 Interacts with Complex I and DAP3 and Regulates Mitochondrial Respiration
850 and Apoptosis. *J Biol Chem*. 2009;284(8):5414-5424. doi:10.1074/jbc.M807797200
- 851 8. Kissil JL, Deiss LP, Bayewitch M, Raveh T, Khaspekov G, Kimchi A. Isolation of DAP3,
852 a Novel Mediator of Interferon- γ -induced Cell Death (*). *Journal of Biological*
853 *Chemistry*. 1995;270(46):27932-27936. doi:10.1074/jbc.270.46.27932
- 854 9. Kissil JL, Cohen O, Raveh T, Kimchi A. Structure-function analysis of an evolutionary
855 conserved protein, DAP3, which mediates TNF-alpha- and Fas-induced cell death. *The*
856 *EMBO Journal*. 1999;18(2):353. doi:10.1093/emboj/18.2.353
- 857 10. Xiao L, Xian H, Lee KY, Xiao B, Wang H, Yu F, Shen HM, Liou YC. Death-associated
858 Protein 3 Regulates Mitochondrial-encoded Protein Synthesis and Mitochondrial
859 Dynamics. *J Biol Chem*. 2015;290(41):24961-24974. doi:10.1074/jbc.M115.673343
- 860 11. Han J, An O, Ren X, Song Y, Tang SJ, Shen H, Ke X, Ng VHE, Tay DJT, Tan HQ, et
861 al. Multilayered control of splicing regulatory networks by DAP3 leads to widespread
862 alternative splicing changes in cancer. *Nat Commun*. 2022;13(1):1793.
863 doi:10.1038/s41467-022-29400-7
- 864 12. Han J, An O, Hong H, Chan THM, Song Y, Shen H, Tang SJ, Lin JS, Ng VHE, Tay
865 DJT, et al. Suppression of adenosine-to-inosine (A-to-I) RNA editome by death
866 associated protein 3 (DAP3) promotes cancer progression. *Sci Adv*.
867 2020;6(25):eaba5136. doi:10.1126/sciadv.aba5136
- 868 13. Faridi R, Rea A, Fenollar-Ferrer C, O'Keefe RT, Gu S, Munir Z, Khan AA, Riazuddin S,
869 Hoa M, Naz S, et al. New insights into Perrault syndrome, a clinically and genetically
870 heterogeneous disorder. *Hum Genet*. Published online August 2, 2021.
871 doi:10.1007/s00439-021-02319-7

- 872 14. Newman WG, Friedman TB, Conway GS, Demain LA. Perrault Syndrome. Published
873 online 2018:19.
- 874 15. Bakhshalizadeh S, Hock DH, Siddall NA, Kline BL, Sreenivasan R, Bell KM,
875 Casagrande F, Kamalanathan S, Sahoo J, Narayanan N, et al. Deficiency of the
876 mitochondrial ribosomal subunit, MRPL50, causes autosomal recessive syndromic
877 premature ovarian insufficiency. *Hum Genet*. Published online May 6, 2023.
878 doi:10.1007/s00439-023-02563-z
- 879 16. Demain L a. m., Antunes D, O'Sullivan J, Bhaskhar S s., O'Keefe R t., Newman W g. A
880 known pathogenic variant in the essential mitochondrial translation gene RMND1
881 causes a Perrault-like syndrome with renal defects. *Clinical Genetics*. 2018;94(2):276-
882 277. doi:10.1111/cge.13255
- 883 17. Menezes MJ, Guo Y, Zhang J, Riley LG, Cooper ST, Thorburn DR, Li J, Dong D, Li Z,
884 Glessner J, et al. Mutation in mitochondrial ribosomal protein S7 (MRPS7) causes
885 congenital sensorineural deafness, progressive hepatic and renal failure and lactic
886 acidemia. *Hum Mol Genet*. 2015;24(8):2297-2307. doi:10.1093/hmg/ddu747
- 887 18. Tucker EJ, Rius R, Jaillard S, Bell K, Lamont PJ, Travessa A, Dupont J, Sampaio L,
888 Dulon J, Vuillaumier-Barrot S, et al. Genomic sequencing highlights the diverse
889 molecular causes of Perrault syndrome: a peroxisomal disorder (PEX6), metabolic
890 disorders (CLPP, GGPS1), and mtDNA maintenance/translation disorders (LARS2,
891 TFAM). *Hum Genet*. 2020;139(10):1325-1343. doi:10.1007/s00439-020-02176-w
- 892 19. Faridi R, Rehman AU, Morell RJ, Friedman PL, Demain L, Zahra S, Khan AA, Tohlob
893 D, Assir MZ, Beaman G, et al. Mutations of SGO2 and CLDN14 collectively cause
894 coincidental Perrault syndrome. *Clin Genet*. 2017;91(2):328-332.
895 doi:10.1111/cge.12867

- 896 20. Sobreira N, Schiettecatte F, Valle D, Hamosh A. GeneMatcher: a matching tool for
897 connecting investigators with an interest in the same gene. *Hum Mutat.*
898 2015;36(10):928-930. doi:10.1002/humu.22844
- 899 21. Wright CF, Fitzgerald TW, Jones WD, Clayton S, McRae JF, van Kogelenberg M, King
900 DA, Ambridge K, Barrett DM, Bayzetenova T, et al. Genetic diagnosis of developmental
901 disorders in the DDD study: a scalable analysis of genome-wide research data. *Lancet.*
902 2015;385(9975):1305-1314. doi:10.1016/S0140-6736(14)61705-0
- 903 22. Smith MJ, Beetz C, Williams SG, Bhaskar SS, O'Sullivan J, Anderson B, Daly SB,
904 Urquhart JE, Bholah Z, Oudit D, et al. Germline mutations in SUFU cause Gorlin
905 syndrome-associated childhood medulloblastoma and redefine the risk associated with
906 PTCH1 mutations. *J Clin Oncol.* 2014;32(36):4155-4161.
907 doi:10.1200/JCO.2014.58.2569
- 908 23. Bauer P, Kandaswamy KK, Weiss MER, Paknia O, Werber M, Bertoli-Avella AM,
909 Yüksel Z, Bochinska M, Oprea GE, Kishore S, et al. Development of an evidence-
910 based algorithm that optimizes sensitivity and specificity in ES-based diagnostics of a
911 clinically heterogeneous patient population. *Genet Med.* 2019;21(1):53-61.
912 doi:10.1038/s41436-018-0016-6
- 913 24. Zech M, Kopajtich R, Steinbrücker K, Bris C, Gueguen N, Feichtinger RG, Achleitner
914 MT, Duzkale N, Périvier M, Koch J, et al. Variants in Mitochondrial ATP Synthase
915 Cause Variable Neurologic Phenotypes. *Ann Neurol.* 2022;91(2):225-237.
916 doi:10.1002/ana.26293
- 917 25. Ellingford JM, Campbell C, Barton S, Bhaskar S, Gupta S, Taylor RL, Sergouniotis PI,
918 Horn B, Lamb JA, Michaelides M, et al. Validation of copy number variation analysis for

- 919 next-generation sequencing diagnostics. *Eur J Hum Genet.* 2017;25(6):719-724.
920 doi:10.1038/ejhg.2017.42
- 921 26. Plagnol V, Curtis J, Epstein M, Mok KY, Stebbings E, Grigoriadou S, Wood NW,
922 Hambleton S, Burns SO, Thrasher AJ, et al. A robust model for read count data in
923 exome sequencing experiments and implications for copy number variant calling.
924 *Bioinformatics.* 2012;28(21):2747-2754. doi:10.1093/bioinformatics/bts526
- 925 27. Frazier AE, Vincent AE, Turnbull DM, Thorburn DR, Taylor RW. Assessment of
926 mitochondrial respiratory chain enzymes in cells and tissues. *Methods Cell Biol.*
927 2020;155:121-156. doi:10.1016/bs.mcb.2019.11.007
- 928 28. Kopajtich R, Smirnov D, Stenton SL, Loipfinger S, Meng C, Scheller IF, Freisinger P,
929 Baski R, Berutti R, Behr J, et al. Integration of proteomics with genomics and
930 transcriptomics increases the diagnostic rate of Mendelian disorders. Published online
931 July 3, 2021:2021.03.09.21253187. doi:10.1101/2021.03.09.21253187
- 932 29. Belyantseva IA. Helios® Gene Gun-Mediated Transfection of the Inner Ear Sensory
933 Epithelium: Recent Updates. In: Sokolowski B, ed. *Auditory and Vestibular Research:
934 Methods and Protocols.* Springer; 2016:3-26. doi:10.1007/978-1-4939-3615-1_1
- 935 30. Yariv B, Yariv E, Kessel A, Masrati G, Chorin AB, Martz E, Mayrose I, Pupko T, Ben-
936 Tal N. Using evolutionary data to make sense of macromolecules with a “face-lifted”
937 ConSurf. *Protein Sci.* 2023;32(3):e4582. doi:10.1002/pro.4582
- 938 31. Gudmundsson S, Singer-Berk M, Stenton SL, Goodrich JK, Wilson MW, Einson J,
939 Watts NA, Consortium GAD, Lappalainen T, Rehm HL, et al. Exploring penetrance of
940 clinically relevant variants in over 800,000 humans from the Genome Aggregation
941 Database. Published online June 13, 2024:2024.06.12.593113.
942 doi:10.1101/2024.06.12.593113

- 943 32. Waterhouse AM, Procter JB, Martin DMA, Clamp M, Barton GJ. Jalview Version 2—a
944 multiple sequence alignment editor and analysis workbench. *Bioinformatics*.
945 2009;25(9):1189-1191. doi:10.1093/bioinformatics/btp033
- 946 33. Itoh Y, Singh V, Khawaja A, Naschberger A, Nguyen MD, Rorbach J, Amunts A.
947 Structure of the mitoribosomal small subunit with streptomycin reveals Fe-S clusters
948 and physiological molecules. Cate JH, Ron D, Croll TI, eds. *eLife*. 2022;11:e77460.
949 doi:10.7554/eLife.77460
- 950 34. Saraste M, Sibbald PR, Wittinghofer A. The P-loop — a common motif in ATP- and
951 GTP-binding proteins. *Trends in Biochemical Sciences*. 1990;15(11):430-434.
952 doi:10.1016/0968-0004(90)90281-F
- 953 35. Sang Y, Yang Q, Guo Y, Liu X, Shen D, Jiang C, Wang X, Li K, Wang H, Yang C, et al.
954 Oocytes orchestrate protein prenylation for mitochondrial function through selective
955 inactivation of cholesterol biosynthesis in murine species. *J Biol Chem*.
956 2023;299(10):105183. doi:10.1016/j.jbc.2023.105183
- 957 36. Khawaja A, Itoh Y, Remes C, Spåhr H, Yukhnovets O, Höfig H, Amunts A, Rorbach J.
958 Distinct pre-initiation steps in human mitochondrial translation. *Nat Commun*.
959 2020;11(1):2932. doi:10.1038/s41467-020-16503-2
- 960 37. Kline BL, Jaillard S, Bell KM, Bakhshalizadeh S, Robevska G, van den Bergen J,
961 Dulon J, Ayers KL, Christodoulou J, Tchan MC, et al. Integral Role of the Mitochondrial
962 Ribosome in Supporting Ovarian Function: MRPS7 Variants in Syndromic Premature
963 Ovarian Insufficiency. *Genes (Basel)*. 2022;13(11):2113. doi:10.3390/genes13112113
- 964 38. Koc EC, Ranasinghe A, Burkhart W, Blackburn K, Koc H, Moseley A, Spremulli LL. A
965 new face on apoptosis: death-associated protein 3 and PDCD9 are mitochondrial

- 966 ribosomal proteins. *FEBS Letters*. 2001;492(1-2):166-170. doi:10.1016/S0014-
967 5793(01)02250-5
- 968 39. Bohnsack MT, Sloan KE. The mitochondrial epitranscriptome: the roles of RNA
969 modifications in mitochondrial translation and human disease. *Cellular and Molecular*
970 *Life Sciences*. 2018;75(2):241. doi:10.1007/s00018-017-2598-6
- 971 40. Chatzisprou IA, Alders M, Guerrero-Castillo S, Zapata Perez R, Haagmans MA,
972 Mouchiroud L, Koster J, Ofman R, Baas F, Waterham HR, et al. A homozygous
973 missense mutation in ERAL1, encoding a mitochondrial rRNA chaperone, causes
974 Perrault syndrome. *Hum Mol Genet*. 2017;26(13):2541-2550. doi:10.1093/hmg/ddx152
- 975 41. Dennerlein S, Rozanska A, Wydro M, Chrzanowska-Lightowlers ZMA, Lightowlers RN.
976 Human ERAL1 is a mitochondrial RNA chaperone involved in the assembly of the 28S
977 small mitochondrial ribosomal subunit. *Biochem J*. 2010;430(Pt 3):551-558.
978 doi:10.1042/BJ20100757
- 979 42. Invernizzi F, Legati A, Nasca A, Lamantea E, Garavaglia B, Gusic M, Kopajtich R,
980 Prokisch H, Zeviani M, Lamperti C, et al. Myopathic mitochondrial DNA depletion
981 syndrome associated with biallelic variants in LIG3. *Brain*. 2021;144(9):e74.
982 doi:10.1093/brain/awab238
- 983 43. van der Ven AT, Cabrera-Orefice A, Wente I, Feichtinger RG, Tsiakas K, Weiss D,
984 Bierhals T, Scholle L, Prokisch H, Kopajtich R, et al. Expanding the phenotypic and
985 biochemical spectrum of NDUFAF3-related mitochondrial disease. *Molecular Genetics*
986 *and Metabolism*. 2023;140(3):107675. doi:10.1016/j.ymgme.2023.107675
- 987 44. Di Nottia M, Marchese M, Verrigni D, Mutti CD, Torraco A, Oliva R, Fernandez-Vizarra
988 E, Morani F, Trani G, Rizza T, et al. A homozygous MRPL24 mutation causes a

- 989 complex movement disorder and affects the mitoribosome assembly. *Neurobiology of*
990 *Disease*. 2020;141:104880. doi:10.1016/j.nbd.2020.104880
- 991 45. Gardeitchik T, Mohamed M, Ruzzenente B, Karall D, Guerrero-Castillo S, Dalloyaux D,
992 van den Brand M, van Kraaij S, van Asbeck E, Assouline Z, et al. Bi-allelic Mutations in
993 the Mitochondrial Ribosomal Protein MRPS2 Cause Sensorineural Hearing Loss,
994 Hypoglycemia, and Multiple OXPHOS Complex Deficiencies. *Am J Hum Genet*.
995 2018;102(4):685-695. doi:10.1016/j.ajhg.2018.02.012
- 996 46. Lake NJ, Webb BD, Stroud DA, Richman TR, Ruzzenente B, Compton AG, Mountford
997 HS, Pulman J, Zangarelli C, Rio M, et al. Biallelic Mutations in MRPS34 Lead to
998 Instability of the Small Mitoribosomal Subunit and Leigh Syndrome. *Am J Hum Genet*.
999 2017;101(2):239-254. doi:10.1016/j.ajhg.2017.07.005
- 1000 47. Prezant TR, Agapian JV, Bohlman MC, Bu X, Öztas S, Qiu WQ, Arnos KS, Cortopassi
1001 GA, Jaber L, Rotter JI, et al. Mitochondrial ribosomal RNA mutation associated with
1002 both antibiotic-induced and non-syndromic deafness. *Nat Genet*. 1993;4(3):289-294.
1003 doi:10.1038/ng0793-289
- 1004 48. Ferrari A, Del'Olio S, Barrientos A. The Diseased Mitoribosome. *FEBS Letters*.
1005 2021;595(8):1025-1061. doi:10.1002/1873-3468.14024
- 1006 49. Singh V, Itoh Y, Del'Olio S, Hassan A, Naschberger A, Flygaard RK, Nobe Y,
1007 Izumikawa K, Aibara S, Andréll J, et al. Structure of mitoribosome reveals mechanism
1008 of mRNA binding, tRNA interactions with L1 stalk, roles of cofactors and rRNA
1009 modifications. *bioRxiv*. Published online July 15, 2023:2023.05.24.542018.
1010 doi:10.1101/2023.05.24.542018
- 1011 50. Hochberg I, Demain LAM, Richer J, Thompson K, Urquhart JE, Rea A, Pagarkar W,
1012 Rodríguez-Palmero A, Schlüter A, Verdura E, et al. Bi-allelic variants in the

- 1013 mitochondrial RNase P subunit PRORP cause mitochondrial tRNA processing defects
1014 and pleiotropic multisystem presentations. *The American Journal of Human Genetics*.
1015 Published online October 2021:S0002929721003797. doi:10.1016/j.ajhg.2021.10.002
- 1016 51. Kim HR, Chae HJ, Thomas M, Miyazaki T, Monosov A, Monosov E, Krajewska M,
1017 Krajewski S, Reed JC. Mammalian dap3 is an essential gene required for
1018 mitochondrial homeostasis in vivo and contributing to the extrinsic pathway for
1019 apoptosis. *The FASEB Journal*. 2007;21(1):188-196. doi:10.1096/fj.06-6283com
- 1020 52. Harada T, Iwai A, Miyazaki T. Identification of DELE, a novel DAP3-binding protein
1021 which is crucial for death receptor-mediated apoptosis induction. *Apoptosis*.
1022 2010;15(10):1247-1255. doi:10.1007/s10495-010-0519-3
- 1023 53. Miyazaki T, Reed JC. A GTP-binding adapter protein couples TRAIL receptors to
1024 apoptosis-inducing proteins. *Nat Immunol*. 2001;2(6):493-500. doi:10.1038/88684
- 1025 54. Maiti P, Kim HJ, Tu YT, Barrientos A. Human GTPBP10 is required for mitoribosome
1026 maturation. *Nucleic Acids Research*. 2018;46(21):11423-11437.
1027 doi:10.1093/nar/gky938
- 1028 55. Maiti P, Lavdovskaia E, Barrientos A, Richter-Dennerlein R. Role of GTPases in driving
1029 mitoribosome assembly. *Trends Cell Biol*. 2021;31(4):284-297.
1030 doi:10.1016/j.tcb.2020.12.008
- 1031 56. Bugiardini E, Mitchell AL, Rosa ID, Horning-Do HT, Pitmann AM, Poole OV, Holton JL,
1032 Shah S, Woodward C, Hargreaves I, et al. MRPS25 mutations impair mitochondrial
1033 translation and cause encephalomyopathy. *Hum Mol Genet*. 2019;28(16):2711-2719.
1034 doi:10.1093/hmg/ddz093

- 1035 57. Jackson CB, Huemer M, Bolognini R, Martin F, Szinnai G, Donner BC, Richter U,
1036 Battersby BJ, Nuoffer JM, Suomalainen A, et al. A variant in MRPS14 (uS14m) causes
1037 perinatal hypertrophic cardiomyopathy with neonatal lactic acidosis, growth retardation,
1038 dysmorphic features and neurological involvement. *Hum Mol Genet.* 2019;28(4):639-
1039 649. doi:10.1093/hmg/ddy374
- 1040 58. Rehm HL, Berg JS, Brooks LD, Bustamante CD, Evans JP, Landrum MJ, Ledbetter
1041 DH, Maglott DR, Martin CL, Nussbaum RL, et al. ClinGen--the Clinical Genome
1042 Resource. *N Engl J Med.* 2015;372(23):2235-2242. doi:10.1056/NEJMs1406261
- 1043